HHS Public Access

Author manuscript

Nat Chem Biol. Author manuscript; available in PMC 2013 October 01.

Published in final edited form as:

Nat Chem Biol. 2013 April ; 9(4): 271–276. doi:10.1038/nchembio.1185.

Allosteric Inhibition of Hypoxia Inducible Factor-2 with Small Molecules

Thomas H Scheuermann[1,2], **Qiming Li**[1], **He-Wen Ma**[1], **Jason Key**[1,2], **Lei Zhang**[1], **Rui Chen**[3], **Joseph A Garcia**[3], **Jacinth Naidoo**[1], **Jamie Longgood**[1], **Doug E Frantz**[1], **Uttam K Tambar**[1], **Kevin H Gardner**[1,2,*], and **Richard K Bruick**[1,*]

[1]Department of Biochemistry, University of Texas Southwestern Medical Center, Dallas, Texas USA

[2]Department of Biophysics, University of Texas Southwestern Medical Center, Dallas, Texas USA

[3]Department of Medicine, Veterans Affairs North Texas Health Care System, and the Department of Internal Medicine, University of Texas Southwestern Medical Center, Dallas, Texas USA

Abstract

Hypoxia Inducible Factors (HIFs) are heterodimeric transcription factors induced in many cancers where they frequently promote the expression of many protumorigenic pathways. Though transcription factors are typically considered “undruggable”, the PAS-B domain of the HIF-2α subunit contains a large cavity within its hydrophobic core that offers a unique foothold for small-molecule regulation. Here we identify artificial ligands that bind within this pocket and characterize the resulting structural and functional changes caused by binding. Notably, these ligands antagonize HIF-2 heterodimerization and DNA-binding activity *in vitro* and in cultured cells, reducing HIF-2 target gene expression. Despite the high identity between HIF-2α and HIF-1α, these ligands are highly selective and do not affect HIF-1 function. These chemical tools establish the molecular basis for selective regulation of HIF-2, providing potential therapeutic opportunities to intervene in HIF-2-driven tumors such as renal cell carcinomas.

Human cells respond to hypoxia through the coordinated actions of the HIF family of transcription factors[1]. Assembled as heterodimers of an oxygen-sensitive subunit (HIF-1α, -2α or 3α) and a dimerization partner (Aryl Hydrocarbon Receptor Nuclear Translocator (ARNT) or HIF-β), these proteins control the expression of hundreds of genes that facilitate cellular adaptation and responses to low oxygen levels[2,3]. While HIFs perform critical physiological functions[1,4,5], increased levels of these potent factors are highly correlated

*Kevin.Gardner@utsouthwestern.edu, Richard.Bruick@utsouthwestern.edu

Author contributions

R.K.B. and K.H.G. conceived and designed the experiments. T.H.S., Q.L., H.-W.M., L.Z., R.C, J.N., and J.L. performed the experiments. R.K.B., K.H.G, T.H.S., J.K., J.A.G., D.E.F, and U.K.T. analyzed the data. R.K.B., K.H.G. and T.H.S. wrote the paper.

PDB code: 4GHI

Competing financial interests

R.K.B., K.H.G., T.H.S., J.K. and U.K.T. have received stock options and other financial compensation from Peloton Therapeutics Inc.

with the onset and progression of a variety of cancers[1]. Indeed, several downstream targets of HIF are well-validated targets for anti-cancer therapies. However, there are potentially significant advantages to directly antagonizing the HIF complexes themselves, and consequently their many downstream targets, as supported by experiments linking HIF ablation to impaired tumorigenesis[6–8]. As such, there is strong interest in the development of artificial compounds to regulate HIF function, to generate both basic research reagents and lead compounds for therapeutic development.

However, HIF presents a traditionally challenging target for pharmacological intervention: it is a large, intracellular protein complex without any active sites that are typically used for small-molecule substrate binding. In addition, much of the transcription factor resides primarily in an extended conformation, further reducing the availability of potential ligand binding sites. However, both HIF subunits contain Per-ARNT-Sim (PAS) protein-protein interaction domains that contribute to the assembly of the HIF complex[9,10] and the recruitment of coactivators[11,12]. These PAS domains are widely used as environmental sensors throughout biology, controlling activities of a diverse array of proteins[13]. Notably, such environmental sensing is often achieved by binding small-molecule cofactors within the core of a PAS domain, using ligand-induced allosteric changes to control the affinity for other protein elements bound to the outside surface[14]. Given the difficulties in directly and selectively antagonizing protein-protein interactions with small molecules[15,16], exploiting such internal cavities offers potential advantages.

The PAS-B domain from HIF-2α appears to be especially amenable to ligand-mediated allosteric regulation. This particular PAS domain contains a relatively large (290 $Å^3$) preformed cavity that can be occupied by either water or by small molecules[17,18]. Using NMR-based screens of small fragment libraries, we have shown that this site can be bound by small-molecule ligands with sub-μM affinities, inducing conformational changes that impair heterodimerization of isolated PAS-B domains *in vitro*[18]. Unfortunately, these molecules were not themselves suitable for further characterization in cultured cells, leading us to use a functionally-based high throughput screen to survey a larger library of more complex compounds for inhibitors capable of disrupting an engineered HIF-2 PAS-B heterodimer.

Here we significantly advance these studies via the development of an improved small-molecule scaffold initially identified in this screen. Biophysical characterization of these compounds, and a derivative optimized by medicinal chemistry approaches, demonstrate specific, selective and efficacious binding within the internal cavity of HIF-2α PAS-B. These compounds disrupt heterodimerization of the full-length HIF-2 transcription factor. Importantly, these molecules function effectively as HIF-2 inhibitors in living cells, disrupting HIF-2 DNA binding and the transcription of its target genes. Moreover, these compounds are selective for the HIF-2 isoform and fail to antagonize HIF-1, whose highly related HIF-1α subunit lacks a comparable ligand-binding site. These reagents provide an opportunity to delineate differences in HIF-1 and HIF-2 physiology and serve as an entry point for eventual selective therapeutic inactivation of HIF-2 in diseases[19], including renal cell carcinomas[20–22].

RESULTS

Identification of HIF-2 PAS-B dimerization antagonists

We previously identified ligands that bind the HIF-2α PAS-B domain using solution NMR-based screening of a small library of almost 800 drug-like fragments[17,18,23]. Following medicinal chemistry optimization, some advanced lead compounds bound HIF-2α with sub-micromolar dissociation constants. Despite their large size (MW~300 Da), these ligands all bound within an internal pocket (290 $Å^3$) completely buried within the HIF-2α PAS-B domain[17,18]. Cavities of this size or larger are quite rare, present in only ~0.3% of over 32,000 high resolution structures of comparably-sized proteins or protein domains (Supplementary Results, Supplementary Fig. 1). Almost all of these cavities constitute ligand-binding sites within the apo- forms of natural ligand binding proteins. Consistent with a comparable functional role for the cavity in HIF-2α PAS-B, our artificial ligands exhibited modest abilities to disrupt isolated PAS-PAS interactions *in vitro*[18]. However, their limited potency to do so limited further characterization in living cells.

To identify superior chemical scaffolds with the potential to antagonize HIF-2 activity in living cells, we developed an *in vitro* assay that assessed functional disruption of PAS-PAS interactions in a high-throughput screening (HTS) format. The isolated wild-type domains associate with a $K_D \approx 100$ μM, precluding many protein-protein interaction assays. This interaction can be improved by more than 100-fold by introducing mutations that enhance ionic interactions at the complex interface without altering other PAS features, including the HIF-2α ligand binding site[18]. These “PAS-B*” variants (R247E HIF-2α and E362R ARNT) were employed in an Amplified Luminescent Proximity Homogeneous Assay (AlphaScreen) to identify compounds capable of disrupting the stabilized heterodimer (Supplementary Fig. 2).

Using this HTS assay, over 200,000 compounds were individually interrogated for their ability to disrupt the HIF-2α-ARNT PAS-B* complex (Supplementary Table 1). The top 640 “hit” compounds, each of which decreased the luminescence proximity signal by over 3σ, were reassayed. Approximately 80% of these initial hits were validated, reflecting the high quality of this screen. However, a large number of these confirmed hits antagonized a key counterscreen designed to eliminate compounds that interfere with the AlphaScreen format itself. Once these nonspecific compounds were eliminated, fewer than 70 candidate disruptors of the HIF-2α-ARNT PAS-B* heterodimer remained. Subsequent titrations of a resupplied subset of these compounds revealed several displaying standard dose-dependent behavior, with IC_{50} values ranging between 0.3 – 10 μM as exemplified for compound (**1**) (Supplementary Fig. 3a,b). Notably, this class of these compounds shared some structural features with amine-linked compounds identified from our NMR-based ligand binding screens[17,18], leading us to further investigate their mode of action and potency.

In principle, the HIF-2α-ARNT PAS-B* heterodimer could be disrupted by small molecules that bound to either of the two PAS-B subunits, either within their cores or at the β-sheet surfaces that mediate protein-protein interactions. Based on the similarity of (**1**) to compounds we previously observed in HIF-2α-ligand complexes[18,23], we anticipated that they might directly bind within the HIF-2α PAS-B* domain. Using NMR spectroscopy to

compare $^{15}N/^{1}H$ HSQC spectra of both PAS-B domains in the absence and presence of (**1**), significant ligand-induced spectral changes were observed for HIF-2α PAS-B, but not for the corresponding ARNT PAS-B subunit (Supplementary Fig. 3c). The slow exchange behavior for these chemical shift changes was consistent with low-μM or tighter dissociation constants. These binding affinities were quantitated using isothermal titration calorimetry (ITC), reporting K_D = 1.1 μM and a 1:1 stoichiometry (Supplementary Fig. 3d), though the high DMSO levels required to solubilize (**1**) likely attenuate the true ligand affinity slightly[17]. In all, there was reasonable correlation between ligand affinity and the sub-μM (~0.4 μM) IC_{50} value observed for heterodimer disruption (Supplementary Fig. 3b).

A medicinal chemistry effort was undertaken to understand the structure-activity relationships underlying the ability of (**1**) to disrupt HIF-2α-ARNT PAS-B* heterodimerization (J.L. Rogers *et al.*, in press; DOI (http://dx.doi.org/10.1021/jm301847z)). An improved analog, (**2**), was identified (Fig. 1a) which also bound to the HIF-2α PAS-B domain (Fig. 1b–d) with a K_D = 81 nM (Fig. 1d). Taken together, these data indicate that this compound class functions by binding directly to HIF-2α.

Antagonists bind within the HIF-2α PAS-B internal cavity

To further define how these compounds disrupt HIF-2α-ARNT PAS-B* heterodimerization, we integrated X-ray crystallographic and high-resolution solution NMR studies of HIF-2α PAS-B bound to compound **(2)**. As anticipated, a co-crystal structure revealed that this ligand bound within the preformed HIF-2α PAS-B internal cavity (Fig. 1a,b; Supplementary Fig. 4 and Supplementary Table 2), displacing water. Compound **(2)** shares some common structural features with the previously described small-molecule ligands (Supplementary Fig. 5), facilitating binding with a combination of van der Waals and electrostatic interactions including: A) placement of ligand nitro group and linker amine adjacent to the H248 imidazole sidechain, B) a pi-hydrogen bond between the Y281 hydroxyl and the A-ring benzene ring, and C) an intra-ligand H-bond shared between the amine linker and the A-ring nitro moiety. Further examination of the structure suggests that compound (**2**) derives its higher affinity from enhanced van der Waals and electrostatic interactions. In particular, the larger di-halogenated Bring of (**2**) better complements the surrounding hydrophobic pocket that was only partially occupied by the B-rings of fragment-derived compounds THS-017, -020 and -044 that bound with 600 nM – 2 μM dissociation constants and lower molar enthalpies[17,18] (Supplementary Fig. 5). In addition, the A-ring of **(2)** presents potential new electrostatic interactions, particularly in placing its oxadiazole ring to H-bond adjacent to one of the S292 sidechain conformations observed in the (**2**) ternary complex. Similarly, identification of B-ring substitutions complementing the apo-protein binding site shape better than (**1**) was key to the development of (**2**) (Supplementary Fig. 5).

Bound ligands induce HIF-2α PAS-B conformational changes

To obtain mechanistic insights of the linkage between small-molecule binding and protein-protein interactions in HIF-2α PAS-B, we compared independent solution and crystallographic data acquired on apo- and (**2**)-bound HIF-2α. The HIF-2α PAS-B-compound (**2**) complex was amenable to high-resolution solution NMR studies (Fig. 1c), allowing us to assign backbone chemical shifts and compare these to existing apo-protein

information[9]. Chemical shift differences observed between these sets (Fig. 2a) established that compound (**2**) binding affected many sites in the surrounding protein, which still retains the mixed α/β PAS domain fold. Mapping these shift changes onto the crystal structure (Fig. 2a,b), we observed many of the largest differences mapping on the β-sheet (particularly the Hβ, Iβ and Aβ strands). Parallel crystallographic analyses used a difference Fourier analysis of apo and (**2**)-bound HIF-2α-ARNT PAS-B* datasets (featuring highly similar crystal parameters) showed ligand-associated changes in electron density both within the HIF-2α cavity and across the neighboring β-sheet (Fig. 2c). Notably, almost no F_o-F_o difference density was observed elsewhere in the structure, including the ARNT PAS-B subunit, providing a powerful control for artifacts from the analysis. These independent analyses link ligand binding to conformational changes at the β-sheet surface of the HIF-2α PAS-B domain that is used to bind its ARNT counterpart (Supplementary Fig. 6), strongly supporting an allosteric mode of action for our artificial inhibitors.

Ligand (2) selectively disrupts HIF-2 heterodimerization

Like (**1**), the conformational changes induced by (**2**) disrupt heterodimerization of isolated HIF-2α and ARNT PAS-B* domains in the AlphaScreen assay (Fig. 3a). However, heterodimerization of the two full-length HIF subunits is mediated by multiple protein-protein interactions involving the PAS-A and basic Helix-Loop-Helix domains[10]. To determine whether (**2**) can antagonize heterodimerization between full length HIF-2α and ARNT polypeptides, we prepared nuclear extracts from hypoxic Hep3B cells. An antibody recognizing the N terminus of ARNT[10], was used to immunoprecipitate the endogenous ARNT protein from the nuclear extracts (Fig. 3b, Supplementary Fig. 7). The HIF-2α subunit co-immunoprecipitated with ARNT in extracts incubated with the DMSO vehicle control. However, addition of (**2**) to the extracts decreased HIF-2α co-immunoprecipitation efficiency by >2-fold in a dose-dependent manner (Fig. 3b). The magnitude of these effects on HIF-2 heterodimerization is similar to that observed following mutation of the HIF-2α PAS-B dimerization interface[10].

In addition to HIF-2α, Hep3B cells also expresses HIF-1α. Though these two HIF-α isoforms share >70% identity between their PAS-B domains, modeling of the HIF-1α PAS-B domain onto the HIF-2α PAS-B structure suggests that several bulkier residues face into the internal HIF-1α cavity (Fig. 4a,b; Supplementary Fig. 8). Such alterations are expected to constrict the pocket and interfere with ligand binding; this was confirmed by ITC data demonstrating that (**2**) effectively does not bind to the HIF-1α PAS-B domain (Fig. 4c; $K_D \gg 5$ μM). The large selectivity of (**2**) for HIF-2α is reflected in Figure 3b, as increasing amounts of (**2**) have little effect on HIF-1 heterodimerization as assessed by co-immunoprecipitation. These data confirm that *in vitro*, (**2**) binds selectively within a preformed ligand binding site buried within the HIF-2α PAS-B domain. Ensuing allosteric conformational changes propagate to the surface of the domain, weakening interactions with the ARNT PAS-B domain and disrupting heterodimerization of the full-length HIF-2 transcription factor.

Ligand (2) selectively disrupts HIF-2 in cultured cells

The improved *in vitro* efficacy of (**2**) provides an opportunity to validate selective HIF-2 antagonism in living cells. No overt toxicity was observed for 786-0 or Hep3B cells incubated with as much as 30 μM of compound (**2**) (Supplementary Fig. 9). The metabolic stability of compound (**2**) when incubated with 786-0 cells *in vitro* was also good, with a $t_{½}$~14 hr; parallel experiments with culture media only demonstrate no loss of compound (**2**) over 24 hr (data not shown). 786-0 cells, derived from a human renal cell carcinoma, lack functional pVHL and constitutively accumulate HIF-2α under normoxic conditions. These cells also lack detectable HIF-1α expression so that HIF-dependent regulation of target genes is attributable to HIF-2 isoform[24]. Addition of (**2**) to cultured 786-0 cells does not alter HIF-2α expression, either at the mRNA (Fig. 5a) or protein levels (Supplementary Fig. 10). However, expression of a well-validated HIF-2 target gene (VEGF) is reduced in a dose-dependent manner in 786-0 cells incubated with (**2**) for 18 hr (Fig. 5a).

To confirm that the mode-of-action for HIF-2 inhibition by (**2**) is indeed dependent upon binding to HIF-2α, we examined ligand effects on Hep3B cells. While some hypoxia inducible target genes are regulated by both HIF-1 and HIF-2 in these cells, other genes are exclusively regulated by a single isoform[25,26]. By examining EPO or PGK1 expression as surrogate markers for HIF-2 and HIF-1, respectively, Hep3B cells were preincubated with 1 or 10 μM (**2**) for 2 hr and maintained either under normoxic or under hypoxic (1% O_2) conditions for 6 or 12 hr. As shown in Figure 5b, while hypoxia induces both EPO and PGK1 mRNA expression, only hypoxic induction of EPO mRNA is antagonized by (**2**). Incubation with (**2**) has no effect on the expression of PGK1 or on the HIF-1α and -2α mRNA levels (Supplementary Fig. 11).

If (**2**) is working in cells by antagonizing HIF-2 heterodimerization, HIF-2's DNA-binding activity should likewise be selectively compromised. Chromatin immunoprecipation (ChIP) using antibodies raised against HIF-1α or HIF-2α was used to measure HIF DNA binding in cultured cells. An increase in both HIF-1 and HIF-2 binding to a HIF-responsive promoter element is observed under hypoxic conditions, reflecting the increase in stability of both α-subunits. However, the DNA-binding activity of HIF-1 is unaffected in cells incubated with 10 μM (**2**) while HIF-2's DNA-binding activity is substantially decreased (Fig. 5c). Together these data constitute a proof-of-principle demonstration that small-molecule ligands can directly and selectively bind to a cavity within the PAS-B domain of the HIF-2α polypeptide. Ligand binding induces conformational changes in HIF-2α that disrupt formation of the HIF-2 heterodimer, antagonizing HIF-2's DNA-binding activity and selectivity reducing expression of HIF-2 target genes in living cells.

DISCUSSION

Great progress has been made in unraveling the relationship between HIF, hypoxia, and tumor progression and metastasis (as reviewed[19,27]). Increased levels of HIF have been observed in human cancers of the brain, breast, kidney and ovaries among others, and are often associated with increased tumor aggressiveness, therapeutic resistance and mortality[27]. While much attention has focused on links between HIF-1α and cancer, there is increasing

evidence that HIF-2α is an important driver of a number of common tumors[19,28]. For example, a clear role for HIF-2 in cancer has been defined for a number of VHL-deficient renal cell carcinomas in which the pro-tumorigenic effects of stabilized HIF-2α cannot be phenocopied by HIF-1α[6–8]. More recently, HIF-2α has been recognized as an intriguing therapeutic target in a number of genetically diverse cancers[29], including glioblastomas[30,31] and nonsmall cell lung carcinomas[32]. The underlying mechanisms responsible for a HIF-2 preference in certain cancers remains the subject of investigation though selectivity in expression, target genes and interaction partners have all been implicated[19].

The accumulation and activity of the HIF-α subunit is acutely induced following a decrease in cellular O_2 levels as is frequently encountered in tumors. Under normoxia, the α-subunit is rapidly degraded following O_2-dependent hydroxylation of key prolines within the oxygen-dependent degradation domain, recruiting the pVHL ubiquitin ligase[33,34]. Parallel O_2-dependent hydroxylation of asparagines in the HIF-α C-terminal transactivation domain also controls HIF's ability to interact with certain transcriptional coactivators[35,36]. However, HIF-α is often constitutively upregulated in an O_2-independent manner in tumors containing appropriate genetic alterations to oncogenic signaling pathways or tumor suppressor genes. This scenario is best exemplified by mutations that inactivate pVHL and result in constitutive stabilization of the HIF-α subunit, predisposing patients to renal cell carcinomas and a host of other cancers[37]. Mutations to many other proteins have also been shown to constitutively-induce HIF-α, albeit by other mechanisms[27]. Small-molecule HIF antagonists that bind directly to the transcription factor, independent of the mechanism underlying its induction, may therefore have utility in a wide range of disease studies.

HIF-2α provides a particularly appealing target for inhibitor development given the preformed cavity present in its PAS-B domain. Such cavities are very rare in protein domains of this size, as they compromise a significant component of the hydrophobic core that normally stabilizes a protein fold. Despite its sequestration from solvent, we have previously shown that this cavity is accessible to small-molecule ligands *in vitro*[17,18]. Here we identify superior compounds that bind to the HIF-2α PAS-B domain with a K_D ~ 80 nM. This class of compounds induces conformational changes within the domain upon binding, with changes identified at the critical β-sheet interface used to bind ARNT PAS-B (Supplementary Fig. 12). Notably, comparable changes are observed in PAS domains with their cognate natural ligands despite differences in ligand structure and activation mechanism, suggesting some degree of conservation in their allosteric activation principles. For example, photosensory PAS domains that bind flavin chromophores comparably to our artificial HIF-2α ligands, harness a change in cofactor configuration via the photochemical formation of a protein-flavin bond to perturb βsheet structure and protein binding[14,38] (Supplementary Fig. 12).

Though multiple protein-protein interactions drive HIF heterodimerization, ligand-dependent allosteric changes to the HIF-2α PAS-B domain are sufficient to disrupt formation of the endogenous full-length HIF-2 complex, with a corresponding selective diminution of HIF-2 activity in living cells. Though HIF PAS domains have been implicated as targets for HIF inihibitors[39,40] this is the first example in which the molecular underpinnings for compound activity have been elucidated. For example, acriflavine was

recently reported to directly antagonize HIF upon binding to the HIF-α PAS-B domains[40]. However, as this compound inhibits both HIF-1 and HIF-2, an internal PAS-B cavity is likely not the relevant binding site as differences among the isoforms confers exquisite specificity.

Though initially charcterized in the context of their role in oxygen sensing, HIFs are responsive to a multitude of cellular cues, including cellular metabilites. For example, the nutrient sensing mTOR pathway acts upstream of HIF-α expression while intermediary metabolites of the Krebs Cycle influence the activity of the HIF hydroxylases[41]. While our findings here provide useful reagents for HIF-2 inhibition, it is tempting to further speculate that such a pocket has evolved for HIF-2 regulation by endogenous metabolites *in vivo*. From a structural perspective, this hypothesis is supported by the presence of rare large cavities (such as in HIF-2α PAS-B) most commonly within apo- forms of natural ligand binding proteins (Supplementary Fig. 1). If so, future elucidation of cognate natural ligands may provide novel insights into isoform-specific metabolic regulation of HIF in physiological and pathological, settings.

ONLINE METHODS

Protein preparation

HIF-2α PAS-B (240-350), HIF-2α PAS-B* (240-350, R247E), ARNT PAS-B (355-470), and ARNT PAS-B* (355-470, E362R) domains were expressed and purified as previously described[18]. HIF-1α PAS-B (238-349) used for ITC and HIF-2α PAS-B used for NMR studies complexed with (**2**) were expressed with an N-terminal Gβ1 fusion tag[23] and purified by Source-Q ion exchange and Superdex S75 size exclusion chromatography. For the HIF-1α PAS-B domain, the Gβ1 tag was not removed, as its retention improved the solubility of the purified PAS-B domain.

AlphaScreen protein reagents were expressed as GST-HIF-2α PAS-B* and His_6-Gβ1-ARNT-PAS-B*-FLAG fusions and purified with affinity (glutathione or Ni(II)) and Superdex S75 chromatography, equilibrated in AlphaScreen assay buffer (50 mM Tris (pH 7.5), 100 mM NaCl; 1 mM dithiothreitol) and flash-frozen in liquid N_2.

NMR analyses

Protein backbone resonance assignments for the HIF-2α PAS-B/compound (**2**) complex were determined using HNCO, HNCACB and CBCA(CO)NH spectra collected on a cryoprobe-equipped Varian Inova 600 MHz spectrometer from a sample of 300 μM U-^{13}C,^{15}N-HIF-2α PAS-B, 350 μM compound **(2)** and 0.4% DMSO in 10 mM d_{11}-Tris pH 7.3, and 20 mM NaCl buffer using NMRViewJ[42]. Data collected at a second condition (5 mM MES, pH 6.5; 20 mM NaCl) were used to resolve ambiguities stemming from exchange broadening in a limited number of sites. Chemical shift differences (Fig. 2a,b) were calculated from backbone HIF-2α PAS-B $^{15}N/^{1}H$ assignments of the complex (here) and apo form[9]:

$$\Delta\delta = \sqrt{\Delta\delta(^1H)^2 + (0.1 * \Delta\delta\,^{15}N)^2}$$

AlphaScreen

Reactions were performed in microtiter plates containing 100 nM GST-HIF-2α PAS-B*, 100 nM ARNT-PAS-B*-Flag, 20 mM Tris-Cl (pH 7.5), 100 mM NaCl, 1 mM DTT, 0.02% Tween-200, 1.5 pg/μl AlphaScreen Glutathione Donor Beads (PerkinElmer), and 1.5 pg/μl AlphaLISA anti-FLAG Acceptor Beads (PerkinElmer). Compound stocks (100X) were prepared in DMSO. Plates were incubated in the dark at room temperature with gentle rocking for 4 hr prior to data collection using an EnVision microplate reader (PerkinElmer). As a control, the individual PAS-B* domains were replaced by a single (doubly-tagged) GST-ARNT-PAS-B*-FLAG protein (230 nM) capable of recruiting both beads to induce an AlphaScreen signal.

NMR ligand binding assay

Compounds were titrated at 125 and 250 μM concentrations into samples of 200 μM uniformly ^{15}N-labeled HIF-2α and ARNT PAS-B domains. Significant changes in peak intensity or locations in ^{15}N/^{1}H HSQC spectra indicated ligand binding.

Isothermal titration calorimetry of protein/small molecule complexes

Thermodynamic parameters of small molecule binding were determined using a MicroCal VP-ITC calorimeter. Protein solutions were extensively dialyzed against buffer (50 mM Tris (pH 7.5), 20 mM NaCl and 5 mM beta-mercaptoethanol), which was subsequently used to prepare a matched compound solution by dilution from a 50 mM compound stock in 100% DMSO. ITC data collected for compound **(1)** were acquired in 5.0% DMSO to improve compound solubility, while data for compound (**2**) was collected at ≤ 0.02% DMSO. Prior controls have demonstrated modest effects of 5% DMSO on measured thermodynamic parameters for HIF/ligand complexes, typically reducing affinities two to four fold[17]. Each isotherm was recorded by injecting 200 μM protein (syringe) into 5 – 10 μM solutions of compound (cell), accounting for dilution heats by subtracting data from a control titration of 200 μM protein into a matched buffer-DMSO solution. Thermograms were fit to a single site binding model to extract equilibrium binding parameters.

Crystallography

Compound **(2)** was co-crystallized as a ternary complex with the HIF-2α/ARNT PAS-B* heterodimer[17,18]. Briefly, HIF-2α/ARNT PAS-B* heterodimers were crystallized in the presence of a stoichiometric excess of (**2**). Ternary complex crystals grew in hanging drops of 2 μl of 300 μM ternary complex and 2 μl of precipitant (100 mM Bis-Tris (pH 5.5–6.0), 20 mM NaCl, 19–23% PEG 3350), which was supplemented with 25% PEG400 prior to freezing in liquid nitrogen. X-ray diffraction data were collected at the Advanced Photon Source (Argonne National Laboratory, Argonne, IL), beamline ID-19 at 100 K using 0.97937 Å X-rays, which were reduced and scaled with the HKL2000 software package[43]. The structures were determined, refined and validated using the PHENIX[44] macromolecular crystallography software suite (version 1.7.2-869) in conjunction with the PRODRG2 web server[45] to generate initial ligand coordinates, molecular modeling with COOT[46], validation with MolProbity[47], and additional analysis and figure preparation in PyMOL (Schrödinger, Inc.). The final structural model was refined with an occupancy of compound **(2)** at 0.7, with

final refinement statistics are presented in Supplementary Table 2 (coordinates deposited at RCSB with PDB code 4GHI). Calculated hydrogen atomic positions were added to protein and ligand coordinate files and employed in a "riding-hydrogen" mode. The final model demonstrates good stereochemical properties, as accessed by Ramachandran (100% favored) and Molprobility (3.17 (98%) clash score and 1.24 (96%) Molprobility scores) analyses. An F_o-F_o electron density difference map (Fig. 2c; Supplementary Fig. 12a) was calculated using difference structure factor amplitudes derived from the apo and ligand-bound diffraction data, with phases derived from the atomic coordinates of the apo protein heterodimer (PDB code: 3F1P[18]). Structure factor amplitudes were scaled using SCALEIT and maps were calculated using FFT, both from the CCP4[48] software suite. The homology model of HIF-1α PAS-B (Fig. 4a,b) was generated with MODELLER[49] using the ligand-free coordinates of HIF-2α PAS-B (3F1P).

Occupancies for sites demonstrating multiple conformers were optimized by phenix.refine including the HIF-2α PAS-B cavity-lining residue M252. As compound (**2**) demonstrates fractional (0.7) occupancy of binding sites in the crystal, both apo (M252-in) and compound (**2**)-bound (M252-out) conformations are represented in $2mF_o$-DF_c density maps (Supplementary Figure 4). The M252-in conformation is not modeled in the final structure for clarity. Fractional occupancy of compound (**2**) is likely a consequence of steric constraints imposed by growing HIF-2α PAS-B*/compound **(2)** crystals under the same conditions previously used grow apo- heterodimer crystals. This approach might constrain compound-induced protein conformational changes associated with PAS-B* heterodimer disruption, reducing HIF-2α PAS-B*/compound affinities and ligand occupancies in the ternary complex.

Buried cavity identification

Solvent-inaccessible cavities were detected and volumes quantitated using an in-house Python-based software program developed specifically for locating internal, buried cavities (available upon request). The program uses a grid-based search to identify regions within the solvent-accessible molecular envelope where a 1.4 Å radius probe sphere, which approximates a water molecule, may be placed without sterically clashing with protein. Adjacent probe-occupied points were iteratively clustered into groups with successively finer grid spacing. At each stage, clusters that extend to the solvent are discarded. Finally, volumes of the contiguous clusters that remain were determined. This approach was applied to a non-redundant subset of the PDB generated based on sequence homology between X-ray crystal structures of 2.5 Å or better resolution (generated by the NCBI VAST tool, non-identical dataset = 32,263 chains as of February 2012). Cavities containing non-water HETATM records, commonly used for ligands and cofactors, were excluded from analysis. This analysis revealed 121,433 cavities with a mean volume of 38.9 $Å^3$.

Cell culture

Human renal adenocarcinoma 786-0 and hepatocellular carcinoma Hep3B cells (AATC) were grown in DMEM/high glucose media (HyClone) supplemented with 10% (786-0) or 15% (Hep3B) fetal bovine serum (Atlanta Biologicals), 20 mM HEPES buffer pH 7.4, 1 mM sodium pyruvate, 100 U/ml penicillin and 100 μg/ml streptomycin (Invitrogen).

Hypoxic experiments performed in a dedicated incubator (Coy Laboratory Products Inc) containing 1% O_2, 5% CO_2 and balance N_2. Compounds were added in DMSO (1% final).

RT-PCR

Cells were collected with Trizol (Invitrogen) and total RNA was extracted using the RNeasy Mini Kit (Qiagen). Following DNase treatment, cDNA was synthesized using SuperScript II Reverse Transcriptase (Invitrogen). Quantitative real time RT-PCR was performed in triplicate using iTaq SYBR Green Supermix with ROX (Bio-Rad) with the 7900HT detection system and software Prism (Applied Biosystems, Inc.). Data were analyzed using the comparative C_T method[50] and expression levels were normalized to cyclophilin B. The data for each gene is the mean of three values determined from three independently harvested sets. The following primers sets were used to amplify Cyclophilin B (TGCCATCGCCAAGGAGTAG; TGCACAGACGGTCACTCAAA), HIF-2α (GCGACAATGACAGCTGACAA; CAGCATCCCGGGACTTCT), EPO (GAGGCCGAGAATATCACGACGGG; TGCCCGACCTCCATCCTCTTCCAG), HIF-1α (TGCCACATCATCACCATATAGAGA; TCCTTTTCCTGCTCTGTTTGG), PGK1 (TTAAAGGGAAGCGGGTCGTTA; TCCATTGTCCAAGCAGAATTTGA), and VEGF1 (CTACCTCCACCATGCCAAGTG; TGATTCTGCCCTCCTCCTTCT).

Co-immunoprecipitation

Nuclear protein extraction and co-IP experiments were performed as previously reported[51]. The following antibodies were used for immunoblot analysis: anti-HIF-1α mouse monoclonal antibody (BD Biosciences); anti-EPAS/HIF-2α mouse monoclonal antibody (Novus Biological); anti-ARNT/HIF-1β mouse monoclonal antibody (Novus Biological).

Chromatin Immunoprecipitation (ChIP)

Experiments were performed as described[52] using the ChIP-IT Express Enzymatic Kit (Active Motif) according to the manufacturer's protocol. ChIP assays were carried out using normal mouse IgG (Santa Cruz Biotechnology), anti-HIF-2α mouse monoclonal antibody (Novus Biologicals), or anti-HIF-1α mouse monoclonal antibody (BD Biosciences). Genomic DNA precipitated from a 15 cm plate cultured in the indicated manner for each treatment, and maintained in parallel to those samples used in gene expression analyses, was analyzed by qPCR using the primers for a human EPO enhancer amplicon (ACTCCTGGCAGCAGTGCAGC; CCCTCTCCTTGATGACAATCTCAGC). The captured genomic DNA was measured by normalizing with that of input material and compared between samples as previously reported[25,52].

786-0 Metabolic Stability Assays

786-0 cells from ATCC (Manassas, VA) were plated at 5000 cells/well in 50 μL in 96-well plates and allowed to adhere overnight in standard RPMI growth media containing 10% FBS, 2 mM glutamine, 1X penicillin streptomycin, 10 mM HEPES, 1 mM sodium pyruvate, and 1X non essential amino acids (all purchased from Life Technologies, Grand Island, NY). Compound (**2**) was dissolved in DMSO at 2 mM, further diluted to 4 μM in HI media, and added to the cells in 50 μL so that the final compound concentration was 2 μM. Two

additional wells containing compound and no cells were plated to serve as time 0 (C_0) and endpoint solvent control (C_{ep}). The cells were then placed in a 37°C, 5% CO_2 incubator. At the timepoints indicated, the media was collected, the cells washed once with PBS and the wash added to the media, and finally the cells were trypsinized and the contents added to the tube containing media and PBS. An equal volume of methanol added to lyse the cells and precipitate proteins. The samples were incubated 10′ at RT and then spun at 15,000× g for 5 min in a microcentrifuge. The supernatant was analyzed by LC-MS/MS. Analytical methods were developed for compound (**2**) using an Applied Biosystems (Foster City, CA) 3200-QTrap, a combination triple quadrupole/ion trap instrument. The parent ion and the two most prominent daughter ions were followed to confirm compound identity, although only the most abundant daughter was used for quantitation. An Agilent (Santa Clara, CA) C18 XDB column, 5 micron packing 50 × 4.6 mm size was used for chromatography.

A modified method[53] was used for determination of metabolic stability half-life by substrate depletion. Briefly, a "% recovered" number was calculated for the C_0 and C_{ep} samples plated in media only to control for compound-related issues such as solubility and stability in the assay media. This value was obtained by dividing C_{ep} LC-MS/MS peak area by the C_0 peak area and multiplying by 100. Typically, acceptable values are between 70-140%[54] although half-lives are reported for compounds with lower % recovered numbers. A "% remaining" value was used to assess metabolic stability of a compound over time. The LC-MS/MS peak area of the incubated sample at each time point was divided by the LC-MS/MS peak area of the time 0 (T_0) sample and multiplied by 100. The natural log (ln) of the % remaining of compound was then plotted versus time (in min) and a linear regression curve plotted going through y-intercept at ln(100). The metabolism of some compounds fail to show linear kinetics at later time point, so those time points are excluded. The half-life ($T_{½}$) was calculated as $T_{½} = 0.693/slope$.

Additional chemical synthetic information and chemical characterization data are provided in the Supplementary Note.

Supplementary Material

Refer to Web version on PubMed Central for supplementary material.

Acknowledgments

The authors thank Shuguang Wang and members of the UTSW HTS Core Facility, Diana Tomchick, Chad Brautigam, John MacMillan, Noelle Williams, and members of our laboratories for their help. This work was funded by grants from the NIH (P01 CA095471, P30 CA142543) and CPRIT (RP-100846). R.K.B. is the Michael L. Rosenberg Scholar in Medical Research and was supported by a Career Award in the Biomedical Sciences from the Burroughs Wellcome Fund; K.H.G. is the Virginia Lazenby O'Hara Chair in Biochemistry and W.W. Caruth Scholar in Biomedical Research; U.K.T. is a W.W. Caruth, Jr. Scholar in Biomedical Research. J.A.G. was supported by funds provided by the Department of Veterans Affairs. Results shown in this report are derived from work performed at Argonne National Laboratory, Structural Biology Center at the Advanced Photon Source. Argonne National Laboratory is operated by UChicago Argonne, LLC, for the U.S. Department of Energy, Office of Biological and Environmental Research under contract DE-AC02-06CH11357. This investigation was conducted in a facility constructed with support from the Research Facilities Improvement Program (Grant # C06 RR 15437-01) from the National Center for Research Resources, National Institutes of Health.

References

1. Semenza GL. Hypoxia-inducible factors: mediators of cancer progression and targets for cancer therapy. Trends Pharmacol Sci. 2012; 33:207–214. [PubMed: 22398146]
2. Xia X, et al. Integrative analysis of HIF binding and transactivation reveals its role in maintaining histone methylation homeostasis. Proc Natl Acad Sci U S A. 2009; 106:4260–4265. [PubMed: 19255431]
3. Schodel J, et al. High-resolution genome-wide mapping of HIF-binding sites by ChIP-seq. Blood. 2011; 117:e207–217. [PubMed: 21447827]
4. Majmundar AJ, Wong WJ, Simon MC. Hypoxia-inducible factors and the response to hypoxic stress. Mol Cell. 2010; 40:294–309. [PubMed: 20965423]
5. Greer SN, Metcalf JL, Wang Y, Ohh M. The updated biology of hypoxia-inducible factor. EMBO J. 2012; 31:2448–2460. [PubMed: 22562152]
6. Kondo K, Kim WY, Lechpammer M, Kaelin WG Jr. Inhibition of HIF2alpha is sufficient to suppress pVHL-defective tumor growth. PLoS Biol. 2003; 1:E83. [PubMed: 14691554]
7. Kondo K, Klco J, Nakamura E, Lechpammer M, Kaelin WG Jr. Inhibition of HIF is necessary for tumor suppression by the von Hippel-Lindau protein. Cancer Cell. 2002; 1:237–246. [PubMed: 12086860]
8. Maranchie JK, et al. The contribution of VHL substrate binding and HIF1-alpha to the phenotype of VHL loss in renal cell carcinoma. Cancer Cell. 2002; 1:247–255. [PubMed: 12086861]
9. Erbel PJ, Card PB, Karakuzu O, Bruick RK, Gardner KH. Structural basis for PAS domain heterodimerization in the basic helix--loop--helix-PAS transcription factor hypoxia-inducible factor. Proc Natl Acad Sci U S A. 2003; 100:15504–15509. [PubMed: 14668441]
10. Yang J, et al. Functions of the Per/ARNT/Sim (PAS) domains of the hypoxia inducible factor (HIF). J Biol Chem. 2005; 280:36047–36054. [PubMed: 16129688]
11. Partch CL, Card PB, Amezcua CA, Gardner KH. Molecular basis of coiled coil coactivator recruitment by the aryl hydrocarbon receptor nuclear translocator (ARNT). J Biol Chem. 2009; 284:15184–15192. [PubMed: 19324882]
12. Partch CL, Gardner KH. Coactivators necessary for transcriptional output of the hypoxia inducible factor, HIF, are directly recruited by ARNT PAS-B. Proc Natl Acad Sci U S A. 2011; 108:7739–7744. [PubMed: 21512126]
13. Henry JT, Crosson S. Ligand-binding PAS domains in a genomic, cellular, and structural context. Annu Rev Microbiol. 2011; 65:261–286. [PubMed: 21663441]
14. Harper SM, Neil LC, Gardner KH. Structural basis of a phototropin light switch. Science. 2003; 301:1541–1544. [PubMed: 12970567]
15. Wells JA, McClendon CL. Reaching for high-hanging fruit in drug discovery at protein-protein interfaces. Nature. 2007; 450:1001–1009. [PubMed: 18075579]
16. Koehler AN. A complex task? Direct modulation of transcription factors with small molecules. Curr Opin Chem Biol. 2010; 14:331–340. [PubMed: 20395165]
17. Key J, Scheuermann TH, Anderson PC, Daggett V, Gardner KH. Principles of ligand binding within a completely buried cavity in HIF2alpha PAS-B. J Am Chem Soc. 2009; 131:17647–17654. [PubMed: 19950993]
18. Scheuermann TH, et al. Artificial ligand binding within the HIF2alpha PAS-B domain of the HIF2 transcription factor. Proc Natl Acad Sci U S A. 2009; 106:450–455. [PubMed: 19129502]
19. Qing G, Simon MC. Hypoxia inducible factor-2alpha: a critical mediator of aggressive tumor phenotypes. Curr Opin Genet Dev. 2009; 19:60–66. [PubMed: 19167211]
20. Morris MR, et al. Mutation analysis of hypoxia-inducible factors HIF1A and HIF2A in renal cell carcinoma. Anticancer Res. 2009; 29:4337–4343. [PubMed: 20032376]
21. Kaelin WG Jr. Treatment of kidney cancer: insights provided by the VHL tumor-suppressor protein. Cancer. 2009; 115:2262–2272. [PubMed: 19402056]
22. Shen C, et al. Genetic and functional studies implicate HIF1alpha as a 14q kidney cancer suppressor gene. Cancer Discov. 2011; 1:222–235. [PubMed: 22037472]

23. Amezcua CA, Harper SM, Rutter J, Gardner KH. Structure and interactions of PAS kinase N-terminal PAS domain: model for intramolecular kinase regulation. Structure. 2002; 10:1349–1361. [PubMed: 12377121]
24. Krieg M, et al. Up-regulation of hypoxia-inducible factors HIF-1alpha and HIF-2alpha under normoxic conditions in renal carcinoma cells by von Hippel-Lindau tumor suppressor gene loss of function. Oncogene. 2000; 19:5435–5443. [PubMed: 11114720]
25. Dioum EM, et al. Regulation of hypoxia-inducible factor 2alpha signaling by the stress-responsive deacetylase sirtuin 1. Science. 2009; 324:1289–1293. [PubMed: 19498162]
26. Scortegagna M, et al. HIF-2alpha regulates murine hematopoietic development in an erythropoietin-dependent manner. Blood. 2005; 105:3133–3140. [PubMed: 15626745]
27. Semenza GL. Targeting HIF-1 for cancer therapy. Nat Rev Cancer. 2003; 3:721–732. [PubMed: 13130303]
28. Keith B, Johnson RS, Simon MC. HIF1alpha and HIF2alpha: sibling rivalry in hypoxic tumour growth and progression. Nat Rev Cancer. 2012; 12:9–22. [PubMed: 22169972]
29. Franovic A, Holterman CE, Payette J, Lee S. Human cancers converge at the HIF-2alpha oncogenic axis. Proc Natl Acad Sci U S A. 2009; 106:21306–21311. [PubMed: 19955413]
30. Holmquist-Mengelbier L, et al. Recruitment of HIF-1alpha and HIF-2alpha to common target genes is differentially regulated in neuroblastoma: HIF-2alpha promotes an aggressive phenotype. Cancer Cell. 2006; 10:413–423. [PubMed: 17097563]
31. Pietras A, et al. HIF-2alpha maintains an undifferentiated state in neural crest-like human neuroblastoma tumor-initiating cells. Proc Natl Acad Sci U S A. 2009; 106:16805–16810. [PubMed: 19805377]
32. Mazumdar J, et al. HIF-2alpha deletion promotes Kras-driven lung tumor development. Proceedings of the National Academy of Sciences of the United States of America. 2010; 107:14182–14187. [PubMed: 20660313]
33. Ivan M, et al. HIFα Targeted for VHL-Mediated Destruction by Proline Hydroxylation: Implications for O_2 Sensing. Science. 2001; 292:464–468. [PubMed: 11292862]
34. Jaakkola P, et al. Targeting of HIF-α to the von Hippel-Lindau Ubiquitylation Complex by O_2-Regulated Prolyl Hydroxylation. Science. 2001; 292:468–472. [PubMed: 11292861]
35. Lando D, et al. FIH-1 is an asparaginyl hydroxylase enzyme that regulates the transcriptional activity of hypoxia-inducible factor. Genes Dev. 2002; 16:1466–1471. [PubMed: 12080085]
36. Lando D, Peet DJ, Whelan DA, Gorman JJ, Whitelaw ML. Asparagine hydroxylation of the HIF transactivation domain: a hypoxic switch. Science. 2002; 295:858–861. [PubMed: 11823643]
37. Kaelin WG. Von Hippel-Lindau disease. Annu Rev Pathol. 2007; 2:145–173. [PubMed: 18039096]
38. Halavaty AS, Moffat K. N- and C-terminal flanking regions modulate light-induced signal transduction in the LOV2 domain of the blue light sensor phototropin 1 from Avena sativa. Biochemistry (Mosc). 2007; 46:14001–14009.
39. Park EJ, et al. Targeting the PAS-A domain of HIF-1alpha for development of small molecule inhibitors of HIF-1. Cell Cycle. 2006; 5:1847–1853. [PubMed: 16861921]
40. Lee K, et al. Acriflavine inhibits HIF-1 dimerization, tumor growth, and vascularization. Proc Natl Acad Sci U S A. 2009; 106:17910–17915. [PubMed: 19805192]
41. Semenza GL. HIF-1: upstream and downstream of cancer metabolism. Curr Opin Genet Dev. 2010; 20:51–56. [PubMed: 19942427]
42. Johnson BA, Blevins RA. NMRView: a computer program for the visualization and analysis of NMR data. J Biomol NMR. 1994; 4:603–614. [PubMed: 22911360]
43. Otwinowski Z, Minor W. Processing of X-ray diffraction data collected in oscillation mode. Methods Enzymol. 1997; 276:307–326.
44. Adams PD, et al. PHENIX: a comprehensive Python-based system for macromolecular structure solution. Acta Crystallogr D Biol Crystallogr. 2010; 66:213–221. [PubMed: 20124702]
45. Schuttelkopf AW, van Aalten DM. PRODRG: a tool for high-throughput crystallography of protein-ligand complexes. Acta Crystallogr D Biol Crystallogr. 2004; 60:1355–1363. [PubMed: 15272157]

46. Emsley P, Cowtan K. Coot: model-building tools for molecular graphics. Acta Crystallogr D Biol Crystallogr. 2004; 60:2126–2132. [PubMed: 15572765]
47. Chen VB, et al. MolProbity: all-atom structure validation for macromolecular crystallography. Acta Crystallogr D Biol Crystallogr. 2010; 66:12–21. [PubMed: 20057044]
48. Winn MD, et al. Overview of the CCP4 suite and current developments. Acta Crystallogr D Biol Crystallogr. 2011; 67:235–242. [PubMed: 21460441]
49. Marti-Renom MA, et al. Comparative protein structure modeling of genes and genomes. Annu Rev Biophys Biomol Struct. 2000; 29:291–325. [PubMed: 10940251]
50. Bookout AL, Mangelsdorf DJ. Quantitative real-time PCR protocol for analysis of nuclear receptor signaling pathways. Nucl Recept Signal. 2003; 1:e012. [PubMed: 16604184]
51. Scheuermann TH, Yang J, Zhang L, Gardner KH, Bruick RK. Hypoxia-inducible factors Per/ARNT/Sim domains: structure and function. Methods Enzymol. 2007; 435:3–24. [PubMed: 17998046]
52. Chen R, Dioum EM, Hogg RT, Gerard RD, Garcia JA. Hypoxia increases sirtuin 1 expression in a hypoxia-inducible factor-dependent manner. J Biol Chem. 2011; 286:13869–13878. [PubMed: 21345792]
53. McNaney CA, et al. An automated liquid chromatography-mass spectrometry process to determine metabolic stability half-life and intrinsic clearance of drug candidates by substrate depletion. Assay Drug Dev Technol. 2008; 6:121–129. [PubMed: 18336089]
54. Drexler DM, et al. An automated high throughput liquid chromatography-mass spectrometry process to assess the metabolic stability of drug candidates. Assay Drug Dev Technol. 2007; 5:247–264. [PubMed: 17477833]

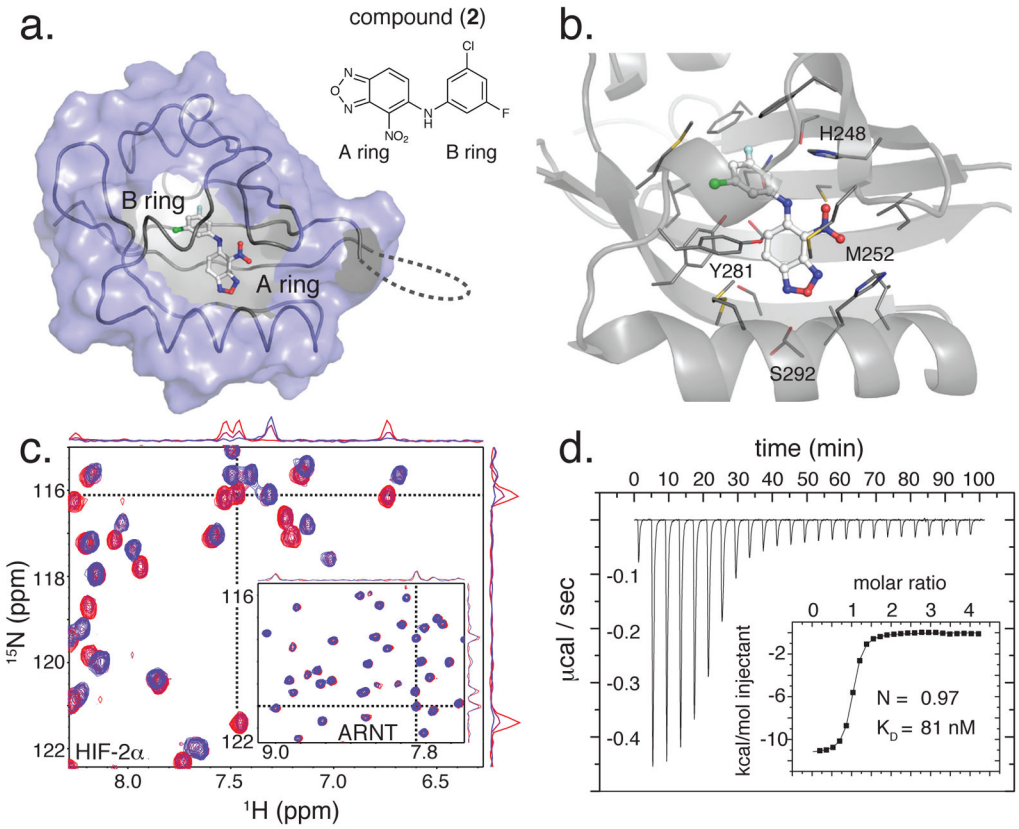

Figure 1. Biophysical characterization of the HIF-2α PAS-B-2 complex

(**a**) The crystal structure of the ternary complex of HIF-2 PAS-B* with compound (**2**) reveals ligand binding into the internal cavity sequestered from bulk solvent within the HIF-2α PAS-B domain (gray). For clarity, the ARNT-PAS-B* portion of the protein heterodimer is not shown, and a portion of the HIF-2α PAS-B* surface (blue) has been cut away to reveal the internal binding site. (**b**) Protein-ligand contacts as revealed by expanded view of the compound **(2)** binding site, showing that it is composed of a mix of polar and hydrophobic residues. (**c**) ^{15}N/^{1}H HSQC spectra of 200 µM ^{15}N HIF-2α PAS-B (main panel) and ^{15}N-ARNT PAS-B (inset) in the presence of 0, 125 and 250µM **(2)** (red to blue) demonstrate the specific binding of compound **(2)** to HIF-2α PAS-B. One-dimensional traces of spectra (at locations shown by dashed lines) demonstrate slow exchange binding behavior of **(2)** to HIF-2α, and no binding to ARNT PAS-B. (**d**) ITC measurements of **(2)** to HIF-2α PAS-B quantitate the binding affinity and 1:1 stoichiometry.

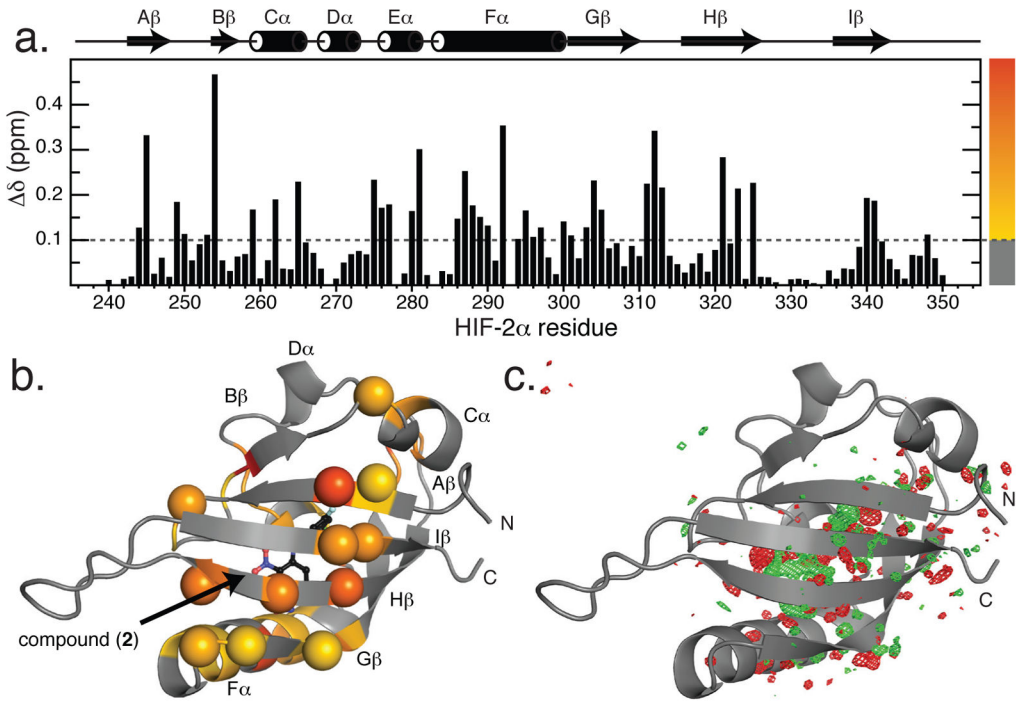

Figure 2. Binding of (2) into HIF-2α PAS-B affects the heterodimeric β-sheet interface between HIF PAS domains

(**a**) Backbone ^{1}H and ^{15}N chemical shift differences between apo-and **(2)**-bound states are mapped onto the HIF-2α PAS-B primary and secondary structures. The yellow-to-red color scale shown on the right is used in (**b**) and Supplementary Figure 6. (**b**) Ligand-induced chemical shift perturbations are mapped onto the HIF-2α PAS-B structure with spheres denoting HIF-2α Cα sites within 8 Å of ARNT PAS-B. View is approximately 180° rotated about the y (vertical) axis from the view in Figure 1a. (**c**) Ligand-induced conformational changes in similar regions are also evident from X-ray diffraction data, as revealed by a F_o(liganded) -F_o(apo) electron density difference map (rendered at 4σ; positive density in green, negative density in red).

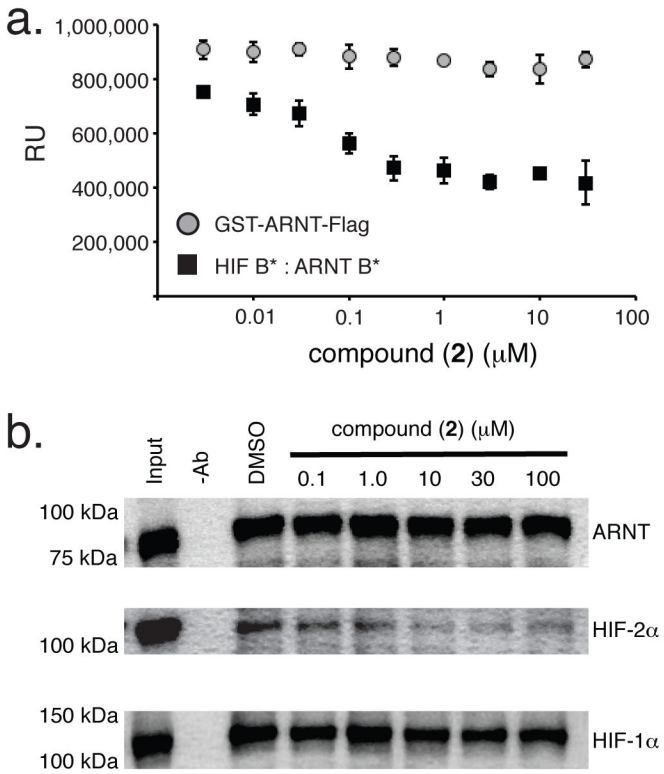

Figure 3. Compound (2) disrupts HIF-2 heterodimerization *in vitro*

(**a**) Addition of (**2**) blocks heterodimer assembly between purified recombinant HIF-2α PAS-B* and ARNT PAS-B* heterodimer (squares) as assessed in the AlphaScreen Assay. No effect was observed in control reactions employing a single (doubly-tagged) GST-ARNT-PAS-B*-FLAG protein capable of recruiting both beads to induce an AlphaScreen signal (circles). Assays were performed in triplicate and the error bars represent ± SD. RU = relative units. (**b**) Compound (**2**) disrupts heterodimerization of the full length HIF-2 transcription factor. Nuclear extracts prepared from hypoxic Hep3B cells expressing ARNT, HIF-1α and HIF-2α (input) were incubated with increasing concentrations of (**2**). Immunoblot analysis indicates amounts of HIF polypeptides immunoprecipitated in the absence (-Ab) or presence of an anti-ARNT antibody.

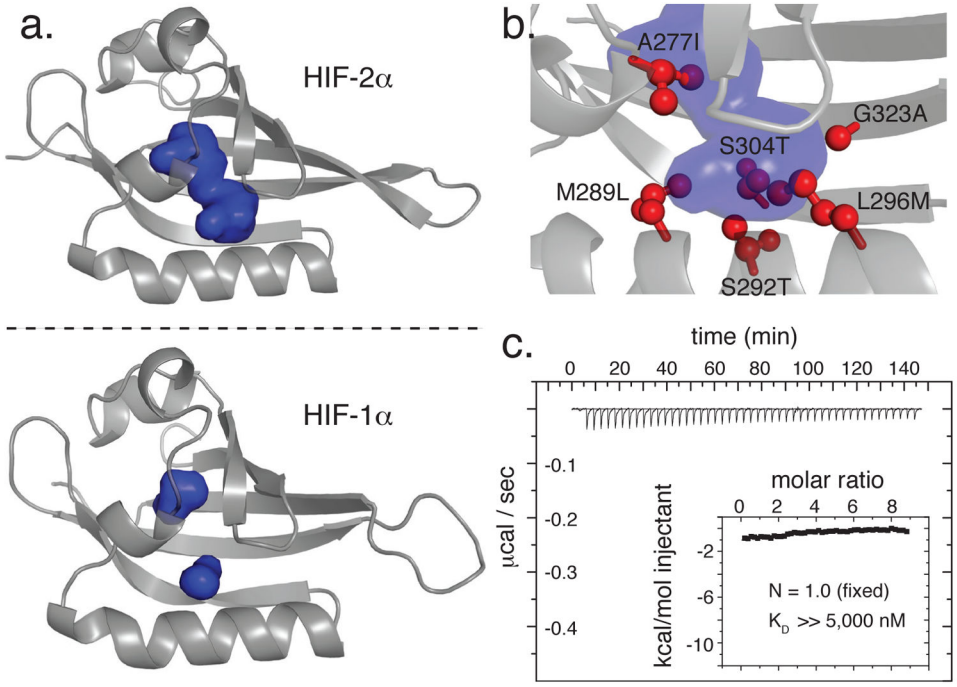

Figure 4. Compound (2) binds selectively to HIF-2α over HIF-1α PAS-B

(**a**) Comparison of internal cavity sizes (blue) identified by a 1.4 Å probe within our HIF-2α PAS-B crystal structure (PDB code 3F1P)[18] (top) and a homology model of HIF-1α PAS-B domain based on this structure. Sequence differences amongst these two closely related paralogs reduce the expected size of the HIF-1α PAS-B cavity. (**b**) The HIF-1α PAS-B model suggests that several sequence differences among these paralogs leads to the placement of bulkier side chains (red) within the HIF-1α PAS-B core. These substitutions appear to shrink the cavity observed in HIF-2α PAS-B (HIF-2α PAS-B cavity rendered as a blue surface, superimposed on the HIF-1α PAS-B model). Amino acid differences are indicated with the first designating HIF-2 amino acid identity, and HIF-1 identity by the last letter. (**c**) ITC measurements of a HIF-1α PAS-B-compound **(2)** titration does not show detectable protein-ligand interaction under the same conditions used to observe binding with HIF-2α PAS-B (Fig. 1d).

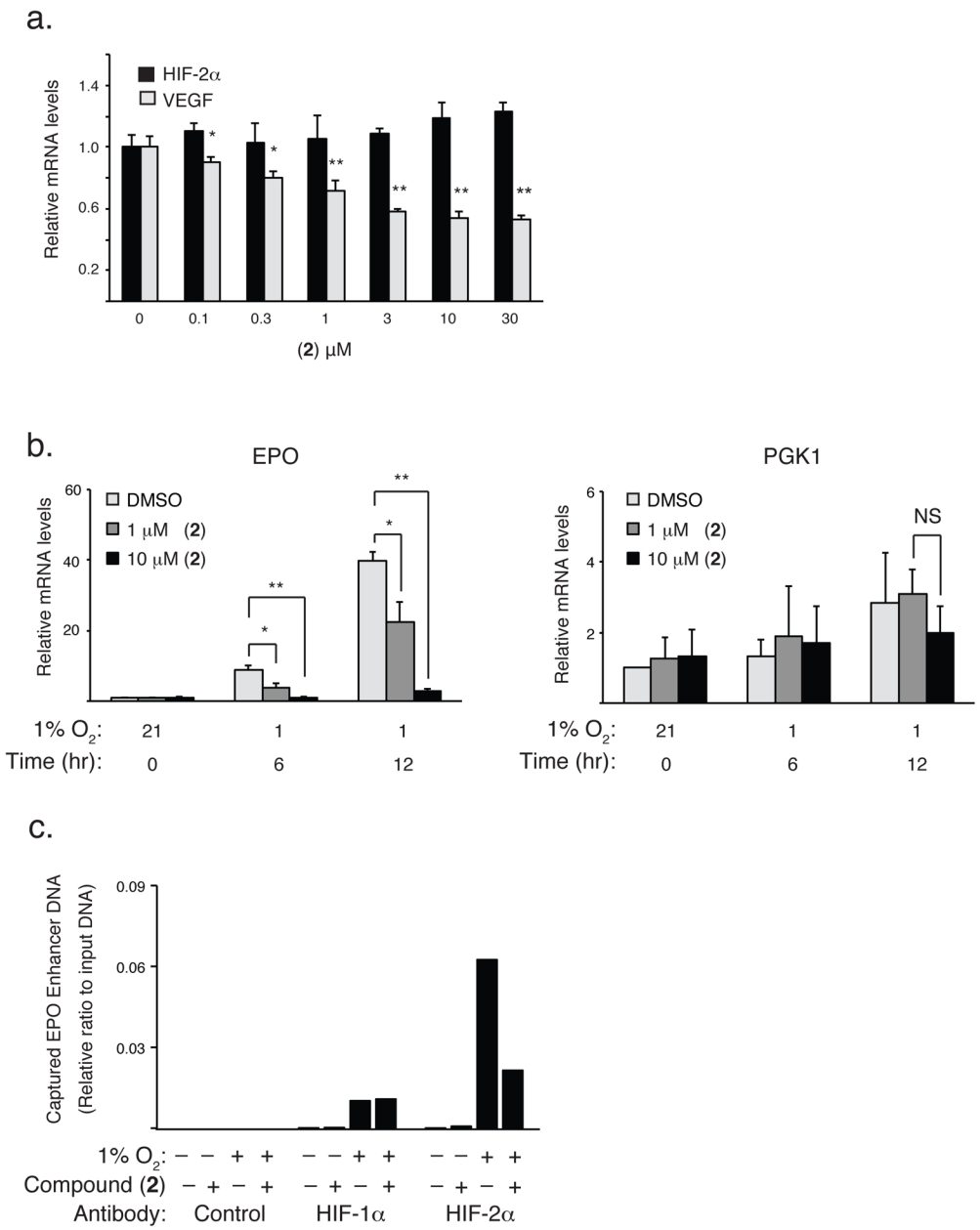

Figure 5. Compound (2) selectively antagonizes HIF-2 activity in cultured cells

While incubation of (**2**) with normoxic 786-0 cells has no effect on HIF-2α expression (**a**), RT-PCR reveals that expression of HIF-2 target genes are antagonized by (**2**) in both 786-0 (**a**) and Hep3B (**b**) cells. (**c**) Compound (**2**) selectively disrupts DNA binding by HIF-2, but not HIF-1, in a ChIP assay. The RT-PCR data for each gene are the mean of three values determined from three independently harvested sets and the error bars represent ± SD. Differences between paired values are statistically significant as determined by t-test. * = $p < 0.01$; ** = $p < 0.001$